Research Article

Title: A deep learning-based multi-modal Detecting-and-Counting-chloroplasts model and its innovative application in complete estimation of chloroplasts in 3D single cells

Qun Su[1,#], Le Liu[2,#], Zhengsheng Hu[1], Tao Wang[8], Huaying Wang[1,8], Qiu-Qi Guo[2], Xinyi Liao[2], Yan Sha[6], Feng Li[9], Zhao Dong[1,5*], Shaokai Yang[6,7*], Ningjing Liu[2*], Qiong Zhao[2,3,4*]

1 School of Mathematics and Physics, Hebei University of Engineering, Handan, Hebei 056038, China

2 School of Life Sciences, East China Normal University, Shanghai 200241, China

3 Institute of Eco-Chongming, Shanghai, China

4 Zhejiang Zhoushan Island Ecosystem Observation and Research Station

5 Hebei Computational Optical Imaging and Photoelectric Detection Technology Innovation Center, Hebei University of Engineering, Handan, Heibei 056038, China

6 University of Alberta, Edomonton, Alberta T6GZE9, Canada

7 Department of Physics, University of Alberta, Edomonton, Alberta T6GZE9, Canada

8 National Satellite Meteorological Centre, Beijing 100081, China

9 The High School Affiliated to Renmin University of China, Beijing 100080, China

# Q. Su and L. Liu contributed equally to the paper.

* Author for Correspondence

Qiong Zhao Email: *qzhao@bio.ecnu.edu.cn*

Zhao Dong Email: *dongzhao@hebeu.edu.cn*

Shao-Kai Yang, *shaokai1@ualberta.ca*

Ning-Jing Liu Email: *liuningjing1@yeah.net*

ORCID

Qun Su https://orcid.org/0009-0005-3512-7276

Le Liu https://orcid.org/0009-0003-9573-2190

Zhengsheng Hu https://orcid.org/0009-0002-1197-329X

Tao Wang https://orcid.org/0009-0006-1245-0510

HuaYing Wang https://orcid.org/0009-0009-9746-0321

Qiu-Qi Guo https://orcid.org/0009-0008-7987-6115

Xinyi Liao https://orcid.org/0000-0002-6562-5541

Yan Sha https://orcid.org/0009-0004-4054-4317

Feng Li https://orcid.org/0009-0003-6964-0030

Zhao Dong https://orcid.org/0000-0002-5849-1979

Shaokai Yang https://orcid.org//0000-0002-7662-6902

Ningjing Liu https://orcid.org/0000-0002-7772-1290

Qiong Zhao https://orcid.org/0000-0003-4557-3139

Total word count (include only Introduction, Materials and Methods, Results and Discussion)	5136	Acknowledgements:	47
Summary:	234	Author contributions	57
Introduction:	1260	No. of figures:	7 (Figs 1-7 in color)
Materials and Methods:	1192	No. of Tables:	1
Results:	1716	No. of Supporting Information files:	11 (Figs S1-S10, Table S1)
Discussion:	968		

Summary

- Detecting-and-Counting-chloroplasts (D&Cchl) is an innovative deep learning-based approach for accurately enumerating chloroplasts in 3D single cells, which is crucial for understanding cell structure, assessing plant growth, studying plant adaptability, and exploring biological evolution.
- This method employs a deep-learning-based object detection algorithm known as You-Only-Look-Once (YOLO), combined with the Intersection Over Union (IOU) strategy. The application of D&Cchl on a single image, or a three-dimensional (3D) volume comprised of a series of images, is efficient in the precise detection and quantification of chloroplasts.
- Expanding on the D&Cchl chloroplast detection model, data from fluorescence microscopy and transmission electron microscopy were used to establish a comprehensive chloroplast multi-modal detection model, which consistently and accurately detected and quantified chloroplasts across various modalities. Single-cell 3D chloroplast counting was successfully implemented by integrating Cellpose, a deep learning-based cell segmentation tool.
- Our model effectively processes public data, requiring no preprocessing or pre-training, and is applicable to various modalities and species. Image annotations have no impact on recognition, demonstrating its reliability. This model provides a powerful tool for chloroplast detection and quantification cross scales, making significant contributions to the intersection of botany and deep learning research.

Key words: Deep Learning; Multi-Modal Detection; Complete Single-Cell 3D Counting; Chloroplasts, D&Cchl Model

Introduction

Chloroplasts convert light energy to chemical energy through photosynthesis, provide oxygen, and act as a cornerstone for the world (Whatley, 1975). The chloroplasts originated approximately 1.5 billion years ago, when a prokaryotic photosynthetic bacterium ancestor was engulfed by a eukaryotic cell in a singular endosymbiotic event (Archibald, 2009; Keeling, 2013). Chloroplasts also contribute to various essential physiological processes including plant growth, development, and environmental adaptation. Studies on chloroplasts mainly focus on its material composition, genome, diversity and evolution, structures, as well as function and adaption (Schubert et al., 2002; van Wijk et al., 2007; Demartini et al., 2011; Gros and Jouhet, 2018; Wakasugi et al., 1997; Gray et al., 1999; Kirchhoff, 2019; Daniell et al., 2016; Cavalier-Smith, 2002; Song et al., 2021; Ouyang et al., 2020). When observed under a microscope, typically, chloroplasts are elliptical or disc-shaped structures, with pigments accumulated inside, resulting in a green color (Murata, 1969; Kume, 2017).

Counting chloroplasts in single cells is critical for understanding cell structure and function, assessing plant growth status, studying plant adaptability and stress resistance, and exploring biological evolution and diversity. Studies showed that the number of chloroplasts might be associated with cell status or function, suggesting a correlation between chloroplast count and plant cell type (Pyke and Leech, 1994; Ii and Webber, 2005). For instance, the reduction in chloroplast number affects both the composition and structure of the photosynthetic apparatus, suggesting that the ability for photosynthesis relies on proper chloroplast division and development (Li and Webber, 2005). Understanding the mechanism of chloroplast number coordination in a specific cell type is a fundamental inquiry. Stomatal guard cells in the plant shoot epidermis typically possess several to tens of chloroplasts per cell (Macfarlane, 1898; Sakisaka, 1929; Mochizuki and Sueoka, 1955; Fujiwara et al., 2019). So far, the number of chloroplasts at the stomatal level

has commonly been utilized as a convenient indicator for identifying hybrid species or estimating the ploidy level of a particular plant tissue (Fujiwara et al., 2019; Watts et al., 2023). Ukwueze et al. investigated the ploidy of banana germplasm through chloroplast counting methods, while Chepkoech et al. (2019) observed an increase in chloroplast numbers in tetraploid potatoes compared to the diploid plant (Ukwueze et al., 2022; Chepkoech et al., 2019). Moreover, Pyke and his colleagues found that the average chloroplast number per cell in the first leaves differs among different genetic backgrounds of *Arabidopsis* (Pyke and Leech, 1994; Pyke et al., 1994). In the Landsberg erecta (Ler) ecotype, the number is 121, while in the Wassilewskija (Ws) ecotype, it is 83 (Pyke and Leech, 1994; Pyke et al., 1994). The above studies suggest the number of chloroplasts can act as a classification marker. Till now, the most commonly used counting methods in the aforementioned studies have been manual counting using images captured via light-microscope, which is time-consuming and prone to misidentification. Molecular staining applied to organelles counting (including chloroplast) associated with flow cytometry may sound high-flux, but it is restricted to the isolation process and cannot accurately determine the number per cell (Mattiasson, 2004; Cole, 2016). Chloroplast counting towards *Spruce needle* leaf showed that detection on the three-dimensional (3D) volume of mesophyll cells, obtained by continuous optical cross-sections via confocal laser-scanning microscopy, provides a wealth of information beyond traditional two-dimensional (2D) images (Kubínová et al., 2014). The authors discovered that nearly 90% of chloroplasts were absent in 2D images compared to the 3D volume when dealing with thick cells (Kubínová et al., 2014). However, this method depends on intricate data collection, which may be impacted by subjectivity and technical limitations. Additionally, studies suggest that semi-automatic cell number quantification can be accomplished using manual-thresholding segmentation and automated measurement with professional software like ImageJ. However, overlapping cells may not be accurately distinguished and counted

(Arena et al., 2017).

As we enter the age of intelligence, deep-learning-based tools in life sciences have become widely utilized. Deep learning, in essence, mimics the learning process of the human brain and has its roots in the study of artificial neural networks. However, due to technological limitations, its progression was stymied for a while. It wasn't until 2012 that the field saw a game-changing moment: Krizhevsky, Sutskever, and Hinton, with their AlexNet, claimed victory in the ImageNet competition, surpassing all other approaches (Krizhevsky, Sutskever and Hinton, 2012). They harnessed the power of GPUs (Graphic Processing Units) for accelerated computation, thereby demonstrating the remarkable potential and efficacy of deep learning in handling large-scale datasets. This breakthrough provided invaluable inspiration to subsequent researchers, catalyzing the widespread adoption of deep learning across a myriad of application domains. Particularly in cell biology, deep learning has unveiled remarkable potential in live cell imaging experiments. Van Valen and his colleagues harnessed the power of deep convolutional neural networks to segment and analyze individual cells in microscopic images, notably achieving high precision in the cytoplasmic segmentation of mammalian cells (Van Valen et al., 2016). In the realm of chemistry, deep learning has paved new pathways for innovative compound design. Utilizing variational autoencoder techniques, scientists have successfully transformed the discrete representations of molecules into continuous multi-dimensional spaces, allowing for the automated generation of innovative chemical structures. This provides a powerful tool for the efficient exploration and optimization of vast chemical compound spaces. (Gómez-Bombarelli et al., 2018). Furthermore, deep learning has been adeptly employed in predicting the sequence specificity of DNA and RNA binding proteins. Leveraging a technique known as DeepBind, researchers are equipped to autonomously discern novel sequence patterns and compute predictive binding scores. Impressively, its performance surpasses that of other existing methods across various experimental

datasets (Alipanahi et al., 2015).

By utilizing convolutional neural networks (CNNs) to estimate the spatial density map of cells, Xie et al. successfully achieved automated cell counting and detection in microscopy images (Xie et al, 2018). Transfer learning and a CNN were combined to analyze over 47,000 confocal fluorescence images from Arabidopsis, resulting in the development of a deep-learning framework called DeeplearnMOR (Deep Learning of the Morphology of Organelles). This tool enables rapid classification of image categories and accurate identification of abnormalities in organelle morphology (Li et al., 2021). An ImageJ plugin that enables non-machine-learning experts to analyze their data with U-Net was provided to solve for frequently occurring quantification tasks such as cell detection and shape measurements in biomedical image data (See http://sites.imagej.net/Falk/plugins/; Falk et al., 2019). You Only Look Once (YOLO) is a popular object detection algorithm that revolutionized the field of computer vision (Redmon and Farhadi, 2016). In YOLO, a single neural network is applied to the entire image, dividing it into grids. This enables YOLO to make real-time predictions with impressive speed, as it only needs a single pass through the network to detect objects in an image, making it an excellent choice for cell detecting and counting (Redmon et al., 2016a; Redmon and Farhadi, 2016; Alam and Islam,2019; Aldughayfiq et al., 2023). However, to the best of our knowledge, there have been no applications of this method to quantify subcellular structures such as chloroplasts or mitochondria using 3D images obtained by optical microscopes from living cells.

Accurate enumeration of chloroplasts is essential for evaluating photosynthetic efficiency and other physiological traits. However, traditional microscopic counting methods are labor-intensive and often lack precision. Here, we developed a YOLOv7-based deep learning tool called Decting&Counting-chloroplast (D&Cchl), integrated with the mode of Intersection Over Union (IOU), for accurate chloroplast counting in multi-types of microscope-captured images. Moreover, we

184 employed the segmentation tool Cellpose to enable counting within individual 3D
185 living cells (Pachitariu and Stringer, 2023). Overall, we achieved the precise
186 complete 3D single cell chloroplast detection and quantification.
187
188
189 **Methods and Materials**
190 **Plant culture**
191 The original bryophyte plant material including *Sphagnum.squarrosum,*
192 *Physcomitrium patens, and Ricciocarpos natans* were gifted by Prof. Ruiliang Zhu
193 and Prof. Yue Sun from the School of Life Sciences at East China Normal
194 University. The original *Wolffia arrhiza* (L.) was gifted by Dr. Li Feng from the
195 High School Affiliated to Renmin University of China.
196 For bryophyte culture, within a clean workbench, the plant's surface soil was first
197 rinsed off with clear water, followed by immersion in a 0.05% Triton buffer solution
198 for 5 minutes. Subsequently, the specimen was treated with a 5% NaClO solution
199 for another 5 minutes and then rinsed with sterilized distilled water three times,
200 each rinse lasting 2 minutes. Excess moisture on the surface of the thallus was
201 absorbed using sterile filter paper. The specimen was then placed on a pre-prepared
202 ½ GB5 medium with 1% sucrose, sealed with a sealing film, and then incubated in
203 a room maintained at a constant temperature of 22℃ with a light cycle of 16 hours
204 (at 800 lux) to 8 hours.
205 For cultivation, thallus sections that were vibrant green and in good growth
206 condition were placed on the same medium for propagation. During this process,
207 the growth status of the scales was observed and documented. The culture medium
208 was prepared by dissolving Gamborg B5 Medium powder and sucrose in distilled
209 water, adjusting the pH to 5.7-5.8, adding agar, and then autoclaving. After
210 sterilization, the medium was poured into Petri dishes and allowed to air-dry at
211 room temperature.

For Arabidopsis Columbia (Col-0, WT) culture, the seedings were transferred to soil 14 days after being cultured on 1/2 Murashige and Skoog (MS) agar medium in a controlled growth chamber (under a condition of 16-h-light/8-h-dark photoperiod, 22° C and 70% relative humidity).

For *Wolffia arrhiza* culture, the plants were cultured in the liquid 1/2 Murashige and Skoog (MS) medium in a controlled growth chamber.

Image collection

In this study, light microscope images of the samples were captured using an Olympus-BX43 biological microscope. Initially, we ensured the microscope slide was clean before adding 3-5 drops of distilled water onto it. Carefully, the liverwort scales were dissected using a dissecting needle and then laid flat in the water droplets on the slide. Once covered with a cover slip, we began our examination under the microscope at a low magnification to initially locate our target. Following this, we switched to a 10×60 high-power magnification for a more detailed observation. After confirming regions where the chloroplasts were relatively dispersed without excessive clustering, photographs were taken, thus yielding a high-quality dataset of chloroplast images, setting the foundation for subsequent analysis. By carefully adjusting the longitudinal translation stage of the sample stage, a series of the microscopic images focused at different depths of the cells were obtained to ensure that all the chloroplasts in the cells could be seen clearly and counted.

The fluorescence microscope images were captured with a LEICA TCS SP8 (Germany) confocal microscope using a 40× or 63× oil immersion objective (excitation wavelengths: 632 nm).

For serial block face scanning electron microscopy (SBF-SEM) imaging, *Sphagnum.squarrosum* capitulum were fixed in a solution of 4% (w/v) paraformaldehyde in PBS at 4 ℃ overnight. The fixed samples were stained with

2% (w/v) osmium tetroxide solution, treated with 1% (w/v) thiocarbohydrazide (TCH) solution, and restained with 1% aqueous uranyl acetate/Walton's lead aspartate solution in turn. Samples were then washed and dehydrated through an ice-cold acetone series (25%, 50%, 75%, 100%, 100%, and 100% acetone) before being embedded in EPIN812 resin at room temperature. Blocks were modified into thin strips, mounted onto a stereomicroscope holder and then imaged and recorded using SEM (3VIEW-SEM, Zeiss). To obtain a three-dimensional image of the sample, a series of images (40 nm per slice) were obtained by removing each slice and imaging the next surface.

Manual labeling for creating the training dataset

In this study, we initially captured approximately 300 bright field light microscopic images, 119 fluorescence microscope images and 512 electron microscope (720*1200) for manual labeling. After selecting images that excelled in terms of resolution, contrast, and chloroplast distribution, we employed the annotation tool, labelimg, to manually label the chloroplasts present in these microscopic images. Utilizing the bounding box feature of this tool, we meticulously assigned a label to each visible chloroplast. In total, we labeled over 20,000 chloroplasts for light microscopic images, 3600 chloroplasts for fluorescence microscope images and 2500 chloroplasts for electron microscope, of which about 90% were used as training data and the remaining 10% served as validation data. The annotated data is typically saved in .txt format, providing precise training and validation datasets for subsequent deep learning training.

Image preprocessing and D&Cchl model training

To run YOLOv7 locally, the appropriate environment needs to be set up first. It's recommended to begin by creating a dedicated Python environment using conda: conda create -n yolov7_env python=3.9, and then activate it with: conda activate

yolov7_env. Within this environment, install the necessary libraries and dependencies using pip install -r requirements.txt. This encompasses the PyTorch deep learning framework and its vision libraries, as well as numerical computation and data processing libraries like numpy, scipy, and pandas, and data visualization libraries such as matplotlib and seaborn. OpenCV is also essential, being a computer vision library used for image processing and visual tasks. Once the dependencies are installed, clone the YOLOv7 project from its GitHub repository (https://github.com/WongKinYiu/yolov7). Proceed with further training or inference after obtaining the source code. Throughout the process, ensure all dependency libraries are correctly installed, and you may need to download pretrained model weights or other resources to run YOLOv7.

We trained the YOLOv7 network for 500, 500, 500 epochs using the Adam optimizer with a learning rate of 0.001 and a batch size of 16 for light microscopic images, fluorescence microscope images and electron microscope individually. The training process lasted 2.662, 2.123 and 3.216 hours for each training. All of our training and testing data were stored in an input directory which contained separate folders for training and testing, along with the corresponding label txt files. Our experiments were conducted on a desktop computer equipped with an Intel Core i7-10700 CPU @ 3.80 GHz and an NVIDIA GeForce RTX 3060 with 12GB of VRAM. The code was executed using the PyTorch 2.0.0 framework and was supported by CUDA version 12.2.

Model performance accuracy analysis

We utilized manually labeled data as the ground truth reference. Any mislabeled or omitted annotations were meticulously counted by human inspection. The accuracy mentioned refers to the proportion of correct annotations made by the artificial intelligence system relative to the manual annotations.

3D volume model reconstruction

Our 3D volume modeling was built upon a series of cell images captured at different focal depths. To construct a comprehensive 3D cell model, we initially captured a sequential set of 2D images from the same sample, with each encompassing distinct depth information of the cell. These consecutive 2D image layers were then arranged in order of their focal depths, and sequentially stacked to form the cohesive 3D cell model. During this process, each 2D layer contributed structural information at a specific depth to the 3D model.

Results

Work frame of the D&Cchl Model for 3D Detection and Quantification of Plant Cell Chloroplasts

To train our model, bright-field images of three bryophyte (*Sphagnum squarrosum* [*S. squ*], *Physcomitrium patens* [*P. pat*], and *Ricciocarpos natans* [*R. nat*]) leaf were obtained under a light microscope (Fig. S1). As ideal plant materials, these plant leaves are single-cell-layered with regular cell distribution (Fig. S1). Totally, 310 pictures (45 of *S. squ*, 56 of *P. pat*, 209 of *R. nat*) were obtained for chloroplast dataset collection. The software LabelImg (See https://github.com/tzutalin/labelImg; Tzutalin, 2015) was used for data pre-treatment to create well-manual-labelled dataset for subsequent model training (Tzutalin, 2015). Then labeled images were fed to the YOLOv7 framework loaded with Yolov7.pt model (Wang et al., 2023). After 500 round 2.662 h training on an NVIDIA GeForce RTX 3060 with 12GB of VRAM, we achieved a new model named D&Cchl (Fig. 1a).

It is generally believed that detecting chloroplasts in 3D space can effectively enhance the precision of chloroplast quantification within cells. In this study, we developed an IOU module to achieve accurate counting within a 3D volume. The module helps reduce repeated counting over a series of 2D images. We set a

threshold value of 0.3 for IOU to measure the overlap between the proposed boxes and the reference boxes. The value of IOU ranges from 0 to 1, indicating the degree of overlap between the detected box and the true label, with 0 indicating no overlap and 1 indicating complete overlap (Fig. 1b). We selected five images from different focal planes as input for three-dimensional (3D) image detection and counting. It's worth noting that during the data collection process, there were almost no lateral shifts in the images during the focusing process. With the assistance of the D&Cchl model, we conducted chloroplast detection and generated detection results for each image. Starting from the first image, all detected chloroplasts were considered as a benchmark. For each subsequent image, the detected chloroplasts were compared with those in the benchmark layer based on their IOU. If the IOU exceeded a preset threshold, it was classified as an existing chloroplast from the benchmark layer, avoiding recounting. Otherwise, it was identified as a new chloroplast and added to the benchmark. The threshold primarily depended on the experiment. If there was minimal lateral image shift during the focusing process, a smaller threshold should be used. Coupled with our proposed IOU method, this approach not only improved potential errors stemming from two-dimensional (2D) image detection but also significantly sped up the processing time compared to manual counting.

Finally, to further enhance the precision and practicality of chloroplast counting within single 3D cell, we employed the Cellpose model to segment the images on a single-cell basis (Fig. 1c). This allowed us to achieve 3D detection and accurate counting of chloroplasts within each cell. By using this advanced technology, we were able to improve the accuracy of our chloroplast counting method significantly. The trained Cellpose model (cyto2) were modified with 11 *R. nat* images to create the suitable model Cyto2Pro, enabling a more detailed and comprehensive analysis of chloroplast distribution within the cells. This breakthrough in chloroplast counting methodology opens up new possibilities for studying the role of chloroplasts in various cellular processes.

The YOLOv7-D&Cchl showed good performance on chloroplast counting and detecting with light microscope 2D images

To thoroughly assess the performance of YOLOv7-D&Cchl in chloroplast detection using light microscope images, we employed the comprehensive evaluation metric, mAP, which combines precision and recall (Figs 2a, S7, S8). In the validation dataset, when the confidence level was set to 0.5, the model achieved an average precision of 0.877. Furthermore, the F1 curve peaked at 0.84, further demonstrating the model's excellent balance between precision and recall (Fig. S9). Additionally, we manually labeled 9 images (3 images from each different plant) with complete chloroplast as a test set to evaluate the efficiency of YOLOv7-D&Cchl in detecting chloroplast (Fig. 1b; Fig. 2b). The model successfully detected 88 chloroplasts in *S. squ* (missing 3), 160 chloroplasts in *P. pat* (missing 10), 194 chloroplasts in *R.nat* (missing 20), and 475 chloroplasts in total images (missing 33), while falsely detected 0 chloroplasts in *S. squ*, 0 chloroplasts in *P. pat*, 0 chloroplast in *R.nat*, and 0 chloroplast in total (Fig. 2c). We also obtained the final counting results and found the precision rates are 97.10%, 96.77%, and 92.72% respectively (Fig. 2d). In all, the D&Cchl model has showed a good performance on chloroplast detecting and counting.

Extended usage of YOLOv7-D&C for chloroplast detecting with light microscope 3D images

We also noticed the mis-detected events and concluded that the white boxes in Fig. 2b and c, due to chloroplasts at different positions not being simultaneously in focus, out-of-focus chloroplasts were not detected by the D&Cch model. To address this issue, a multilayer of light-microscope images covering a whole cell was collected (Figs 1b, 3). To avoid duplicate counting, IOU calculations were performed between each detected target in the second image and the targets in the benchmark. The maximum value was selected and compared to the predetermined IOU

threshold (set at 0.3). If the IOU exceeded the preset threshold, it was classified as an existing chloroplast in the benchmark to prevent duplicate counting, otherwise, it was identified as a new chloroplast and added to the benchmark (Fig. 3). Sequenced images of *S. squ*, *P. pat*, and *R.nat* leaf cells were obtained at various focal depths (Fig. 3a). YOLOv7-D&Cchl was applied for each individual layer, and IOU was used for monitor the overlaps of every target between layers. The accurate counts of chloroplasts in different plants were obtained, with the counts being 326, 184, and 365, respectively. The precision was significantly improved in multilayer statistics than that in the single-layer image, as only about 90% percentage of total chloroplasts could be detected in a single-layer image compared to total multilayer images. Usually, scientists performed chloroplast detecting using single-layer image, because it is exceedingly difficult and time-consuming to get rid of repeated chloroplast counting in multilayer images (Grishagin, 2015). We compared the efficiency of manual detection and counting for multilayer images with the YOLOv7-D&Cchl-mediated chloroplast detection and counting, and concluded that our strategy obviously saves more time than the manual method. Furthermore, after resolving the out-of-focus issue, instances of mis-detection by YOLOv7-D&Cchl were practically eliminated. Thus, our 3D detecting and counting method not only addresses the counting errors caused by severe out-of-focus and defocusing issues in 2D counting but also significantly enhances efficiency, which is particularly meaningful for studying organelles within whole cells.

3D Chloroplast Detection towards different types of images Using the YOLOv7-D&Cchl Model

In the extended application of the YOLOv7-D&Cchl model for 3D detection, we also incorporated various types of images to demonstrate the method's universality. Specifically, we conducted 3D chloroplast detection towards different types of images, including fluorescent microscope images from *Arabidopsis thaliana* [*A.tha*]

rosette leaves, electron microscopy images of *Sphagnum squarrosum* [*S.squ*] leaves. The same training strategies were used on various types of images, similar to those used for light microscope imagery.

To ensure clarity and avoid confusion among the various models, the original YOLOv7-D&Cchl designed for light microscope images was renamed as YOLOv7-D&Cchl_L. Similarly, the model specifically trained for the detection of EM data was designated as YOLOv7-D&Cchl_E. Additionally, the model trained for fluorescent images was named YOLOv7-D&Cchl_F. These nomenclatural changes aim to establish a consistent and systematic naming convention that reflects the unique capabilities and applications of each model.

To assess the performance of these models, we conducted tests on three distinct sets of untreated images (Figs 4, S2). The results revealed that 66, 5, and 73 chloroplasts were individually identified from fluorescent, electron microscopy (EM), and light microscope images, respectively. Notably, for the light microscope images, we purposely utilized a set from multilayer cell leaves of *W. arr*, which exhibited inferior clarity compared to single-layered cell images (Fig. 4). These results not only affirm the high adaptability and precision of the YOLOv7-D&C model in chloroplast detection and counting across various types and complexities of images, but also underscore the capability of deep learning methods in precise organelle quantification within diverse biological samples, highlighting their potential and universality in biological research.

Association of YOLOv7-D&C with cell segmentation for chloroplast detecting in single 3D cell

Bio-scientists find single-cell counting to be more meaningful than counting based solely on single 2D images. Therefore, we employed a segmentation method, segmenting the data obtained from optical microscopy on a single-cell basis, and then carried out automatic segmentation. The pre-trained model ‘cyto2’ loaded into

436 the segmentation tool *Cellpose* has been employed and slightly tuned for the cell
437 segmentation. We re-trained the original model cyto2 with our dataset and obtained
438 a new model named 'cyto2pro', and then utilized it to segment optical microscope
439 images. We specifically chose intact individual cells as inputs for object detection,
440 subsequently conducting chloroplast detection and counting within those individual
441 cells. Single cells were segmented and numbered sequentially. As shown in Fig. 5b,
442 chloroplasts were detected and counted in 4 cells. The numbers of chloroplasts
443 detected in these cells were 24, 28, 37, and 25, respectively, for 2D detection. While
444 conducting multi-layer counting at the 3D level, the results per cell were 35, 36, 51,
445 and 32, respectively. Therefore, we can conclude that our 3D whole cell counting
446 methods provide a more accurate reflection of chloroplast status in cells.
447 Together, we developed the YOLOv7-D&Cchl as an excellent tool for chloroplasts
448 counting. We also propose and utilize the IOU module to solve the duplication issue
449 for counting multilayer-image stacks. Finally, with the integration of the cell
450 segmentation tool Cellpose, single cell 3D counting has become a reality. This
451 solution effectively addresses the challenges faced by our bio-scientists.
452
453 **Exceptional performance of YOLOv7-D&Cchl model on external public data**
454 To validate the universality of our proposed chloroplast counting method, we
455 conducted an experiment where we randomly selected images from external public
456 data, without any preprocessing. As illustrated, the results are presented in two rows:
457 the first row shows the input images, and the second row shows the output images
458 (Fig. 6). It can be observed that our method is still capable of effectively detecting
459 chloroplasts even without preprocessing. This demonstrates the robustness and
460 universality of our method in handling actual unknown data. For image sources,
461 refer to Table S1.
462
463 **Discussion**

The potential application of the D&C in plant cells

The innovative approach of D&Cchl has paved new avenues for plant cell research. Its potential applications extend to various fields in botany and cellular biology. Precise quantification of chloroplasts within plant cells can provide valuable insights into a plant's photosynthetic capacity, growth, and developmental stages (Xiong et al., 2017; Fujiwara et al., 2019). By thoroughly understanding the quantity and distribution status of chloroplasts in different plant species or under varying environmental conditions, researchers can gain a deeper understanding of photosynthesis efficiency and the underlying factors behind it. Additionally, plants often undergo morphological changes during developmental process, as well as in response to environmental stresses like drought, extreme temperatures, or high light intensities, including adjustments in chloroplast distribution (Zahra et al., 2022; Liu et al., 2018; Feng et al., 2019). Monitoring the number and distribution of chloroplasts in plant cells using D&Cchl benefits researchers by providing easy access to information regarding the plants' status, growth rate, and developmental phase. Additionally, it helps in identifying environmental responses and understanding a plant's adaptability to changing conditions.

Our D&Cchl can be widely utilized for its convenient data collection

Currently, there are four main counting methods that are widely used, as depicted in Fig. 7a and Table 1: manual counting, semi-automated counting, deep-learning-based DeepLearnMOR (Li et al., 2021), and the proposed D&Cchl. Manual counting is a straightforward method, but it is time-consuming, labor-intensive, and susceptible to counting errors. For example, the ImageJ/Fiji provides several robust suite of counting tools, such as cell Counter (Plugins-Analyze-Cell Counter), to assist with manual labeling and auto-numbering (Arena， er al., 2017). Semi-automated counting often requires user intervention and parameter configuration for image segmentation and object counting. For instance, the ImageJ/Fiji Analyze

Particles (Analyze-Analyze Particles) allows one-click counting relying on image pre-treatment using threshold-based segmentation (Rueden et al., 2017; Schneider, er al., 2012), to ensure precision and dependability. However, it's important to note that ImageJ has limitations in terms of counting accuracy, and it lacks batch processing capabilities. It can only process images one at a time. This single-image processing method may become time-consuming and less convenient when dealing with large-scale data analysis. DeeplearnMOR was developed based on YOLOv5 (YOLO version 5) for counting chloroplasts in fluorescent images. This approach offers the advantages of high precision and speed in two-dimensional object detection, as well as achieving full automation in counting. However, the requirement of fluorescent images narrowed the practicability. Our proposed method for counting chloroplasts in 3D single cells not only achieves high accuracy, but also is versatile across various chloroplasts from unlimited plant species. As described in Fig. 7b and 7c, the 2D or 3D images captured via optical microscopes undergo **Cellpose** for cell segmentation and **YOLOv7-D&Cchl** for auto-detecting and counting (Fig. 7b, c). By utilizing this approach, we were able to achieve automated counting of chloroplasts, which has the potential for widespread use due to its straightforward data requirements.

Currently, we have successfully trained three distinct chloroplast detection models for images collected from light microscopy, fluorescence microscopy, and electron microscopy, respectively. These models demonstrate superior performance within their designated scopes of application. Nonetheless, a noteworthy impediment to their widespread adoption lies in the prerequisite of specialized knowledge required for their selection and operation. To address this challenge, it is imperative to develop a multimodal model that can adaptively process a diverse array of microscope imagery. We propose to integrate the classification and detection capabilities of YOLO to develop a unified model that can automatically recognize and process different microscope images. By leveraging YOLO, we can categorize

and enumerate chloroplasts through the meticulous classification of all entities and the application of distinct labels. Furthermore, the synergistic integration of deep convolutional networks, such as VGG (Simonyan and Zisserman, 2014), with its profound architecture and exceptional feature extraction capabilities, can significantly bolster the classification accuracy of the model. The seamless integration of YOLO's rapid detection abilities with VGG's profound feature extraction enables the creation of an efficient model that can swiftly locate chloroplasts and precisely discern between various microscope modalities. This multimodal model not only streamlines the operational workflow but also facilitates seamless analytical transitions between distinct microscope technologies, thereby enhancing productivity and enhancing user experience. Consequently, future research endeavors should prioritize the harmonious integration of diverse detection and classification techniques to construct an efficient, accurate, and user-friendly chloroplast image analysis system. This will further enhance the model's adaptability and flexibility, ensuring high-quality analytical outcomes across a range of observation scenarios.

Extended usage of D&C associated with other deep learning-based tools

The D&Cchl method, rooted in the power of deep learning, offers a revolutionary solution for accurately counting chloroplasts in plant cells. Its value becomes even more significant when considering its potential synergy with other deep learning techniques. By integrating with object detection frameworks like Faster R-CNN (Faster Region-CNN) or SSD (Single Shot MultiBox Detector), D&Cchl can enhance the precision and segmentation accuracy of chloroplasts (Liu W et al.,2016; Girshick R et al.,2015). When paired with time series analysis tools like LSTM (Long Short-Term Memory), it becomes possible to monitor the dynamics of chloroplasts within plant cells across various environmental conditions in real-time (Hochreiter and Schmidhuber,1997). Furthermore, combining multimodal data

such as spectral images and thermal imaging provides a comprehensive insight into the health status of plants. With the addition of technologies like autoencoders and VAEs (Variational Autoencoders), deep extraction of cellular features from microscopic images becomes feasible. In essence, the amalgamation of these technologies offers a more efficient and holistic approach to plant cell research.

In summary, different counting methods present their own merits and complexities. Our proposed approach overcomes the limitations of other techniques by harnessing the capabilities of deep learning and integrating various methodologies to achieve precise and comprehensive counting, offering a powerful tool for biological research.

Acknowledgement

This research received support from the Natural Science Foundation of Hebei Province (No. F 2023402009), East China Normal University, the National Natural Science Foundation of China (Grant No. 62175059), and the Multi-modal cross-scale Biomedical Imaging Facility Early bird 2.0 projects from Peking University National Biomedical Imaging Center.

Author contributions

Q.Z, Z.D, S.K, N.J.L and S.Q. designed most of the experiments. S.Q and L.L performed most of the experiment. L.L, Q.Q.G, X.Y.L and F. L performed the plant material culture and collected image data. W.T, H.Z.S, W.H.Y and Y.S assisted the workstation or platform preparation or others. Q.S, Z.D, N.J.L, S.K, and Q.Z wrote the manuscript and conceived the research.

Data availability

The data underlying this article are available in the article and in its online supplementary material. The raw dataset, as well as the scripts for the D&Cchl

model training and application macro, were shared on GitHub https://github.com/Shaokai9/AI4LifeScience_ECNU/tree/main/Deep%20subcellular%20detection.

References

Aldughayfiq B, Ashfaq F, Jhanjhi NZ and Humayun M. 2023. YOLOv5-FPN: A Robust Framework for Multi-Sized Cell Counting in Fluorescence Images. *Diagnostics* **13**: 2280.

Alam MM and Islam MT. 2019. Machine learning approach of automatic identification and counting of blood cells. Healthcare Technology Letters. 6: 103-108.

Alipanahi B, Delong A, Weirauch M.T et al. 2015. Predicting the sequence specificities of DNA- and RNA-binding proteins by deep learning. *Nature Biotechnology* **33(8)** : 831-838.

Arena ET, Rueden CT, Hiner MC, Wang S, Yuan M and Eliceiri KW. 2017. Quantitating the cell: turning images into numbers with ImageJ. *Wiley Interdisciplinary Reviews: Developmental Biology* **6**: e260.

Archibald JM. 2009. The puzzle of plastid evolution. *Current Biology*. 19: R81–R88.

Cavalier-Smith T. 2002. Chloroplast evolution: secondary symbiogenesis and multiple losses. *Curr Biol* 12**:** R62-4.

Chepkoech E, Kinyua MG, Kiplagat OK, Ochuodho JO, Bado S, Kinyua Z, Kimno S and Chelulei M. 2019. Assessment of the Ploidy Level Diversity by Chloroplast Counts in Stomatal Guard Cells of Potato (Solanum tuberosum L.) Mutants. *Asian Journal of Research in Crop Science* **4**: 1-7.

Cole LW. 2016. The evolution of per-cell organelle number. *Frontiers in Cell and Developmental Biology* **4**: 85.

Daniell H, Lin CS, Yu M and Chang WJ. 2016. Chloroplast genomes: diversity,

evolution, and applications in genetic engineering. *Genome Biol* **17**: 134.

Demartini DR, Carlini CR and Thelen JJ. 2011. Proteome databases and other online resources for chloroplast research in Arabidopsis. *Methods Mol Biol* **775**: 93-115.

Falk T, Mai D, Bensch R, Çiçek Ö, Abdulkadir A, Marrakchi Y, Böhm A, Deubner J, Jäckel Z and Seiwald K et al. 2019. U-Net: deep learning for cell counting, detection, and morphometry. *Nature Methods* **16**: 67-70.

Feng L, Raza MA, Li Z, Chen Y, Khalid MHB, Du J, Liu W, Wu X, Song C, Yu L, Zhang Z, Yuan S, Yang W and Yang F. 2019. The Influence of Light Intensity and Leaf Movement on Photosynthesis Characteristics and Carbon Balance of Soybean. *Front. Plant Sci* **9**:1952.

Free software: MIT license Citation: Tzutalin. 2015. LabelImg. Git code. https://github.com/tzutalin/labelImg

Fujiwara MT, Sanjaya A and Itoh RD. 2019. Arabidopsis thaliana leaf epidermal guard cells: a model for studying chloroplast proliferation and partitioning in plants. *Frontiers in Plant Science* **10**: 1403.

Girshick R, Donahue J, Darrell T, et al. 2015. Region-based Convolutional Networks for Accurate Object Detection and Segmentation. *IEEE/CVF Conference on Computer Vision and Pattern Recognition (CVPR)* pp: 142-158.

Gómez-Bombarelli R Wei, J. N Duvenaud D et al. 2018. Automatic chemical design using a data-driven continuous representation of molecules. *ACS Central Science* **4(2)** : 268-276.

Gray MW. 1999. Evolution of organellar genomes. *Curr Opin Genet Dev*. 9: 678-87.

Grishagin, I. V. 2015. Automatic cell counting with ImageJ. *Analytical Biochemistry* **473**:63-65.

Gros V and Jouhet J. 2018. Quantitative Assessment of the Chloroplast Lipidome. *Methods Mol Biol* **1829**: 241-252.

632 Hochreiter S and Schmidhuber J. 1997. Long short-term memory. *Neural*
633 *computation* **9(8)**: 1735-1780.
634 Ii JA and Webber AN. 2005. Photosynthesis in Arabidopsis thaliana mutants with
635 reduced chloroplast number. *Photosynthesis Research* **85**: 373-384.
636 Keeling PJ. 2013. The number, speed, and impact of plastid endosymbioses in
637 eukaryotic evolution. Annu. Rev. *Plant Biol* **64**: 583–607.
638 Kirchhoff H. 2019. Chloroplast ultrastructure in plants. *New Phytol* **223**: 565-574.
639 Krizhevsky A, Sutskever I, Hinton G. E. 2012. ImageNet classification with deep
640 convolutional neural networks. *In Advances in Neural Information Processing*
641 *Systems* **25**.
642 Kubínová Z, Janáček J, Lhotáková Z, Kubínová L and Albrechtová J. 2014.
643 Unbiased estimation of chloroplast number in mesophyll cells: advantage of a
644 genuine three-dimensional approach. *Journal of Experimental Botany* **65**: 609-620.
645 Kume A. 2017. Importance of the green color, absorption gradient, and spectral
646 absorption of chloroplasts for the radiative energy balance of leaves. *J Plant Res*
647 **130**: 501-514.
648 Li J, Peng J, Jiang X, Rea AC, Peng J and Hu J. 2021. DeepLearnMOR: a deep-
649 learning framework for fluorescence image-based classification of organelle
650 morphology. *Plant Physiol* **186**: 1786-1799.
651 Liu, W. et al. 2016. SSD: Single Shot MultiBox Detector. In: Leibe, B., Matas, J.,
652 Sebe, N., Welling, M. (eds) Computer Vision – ECCV 2016. ECCV 2016. *Lecture*
653 *Notes in Computer Science* vol **9905**: Springer, Cham.
654 Liu X, Zhou Y, Xiao J and Bao F. 2018. Effects of Chilling on the Structure,
655 Function and Development of Chloroplasts. Front. *Plant Sci* **9**:1715.
656 Li J, Peng J, Jiang X, Rea AC, Peng J, Hu J. 2021. DeepLearnMOR: a deep-learning
657 framework for fluorescence image-based classification of organelle morphology.
658 *Plant Physiol* **186**:1786-1799.
659 Macfarlane J.M. 1899. Observations on some hybrids between Drosera filiformis

and D. intermedia. *Transactions and Proceedings of the Botanical Society of Pennsylvania* **1:** 87–99.

Mattiasson G. 2004. Flow cytometric analysis of isolated liver mitochondria to detect changes relevant to cell death. *Cytometry Part A: The Journal of the International Society for Analytical Cytology* **60(2)**: 145-154.

Mochizuki A, Sueoka N. 1955. Genetic studies on the number of plastid in stomata I. Effects of autopolyploidy in sugar beets. *Cytologia* **20**: 358–366.

Murata N. 1969. Control of excitation transfer in photosynthesis. II. Magnesium ion-dependent distribution of excitation energy between two pigment systems in spinach chloroplasts. *Biochim Biophys Acta* **189**: 171-81.

Ouyang M, Li X, Zhang J, Feng P, Pu H, Kong L, Bai Z, Rong L, Xu X and Chi W. 2020. Liquid-Liquid Phase Transition Drives Intra-chloroplast Cargo Sorting. *Cell*. **180:** 1144-1159.e20.

Pachitariu M and Stringer C. 2022. Cellpose 2.0: how to train your own model. *Nature Methods* **19**: 1634-1641.

Pyke KA and Leech RM. 1994. A genetic analysis of chloroplast division and expansion in Arabidopsis thaliana. *Plant Physiology* **104**: 201-207.

Pyke KA, Rutherford SM, Robertson EJ and Leech RM. 1994. arc6, A Fertile Arabidopsis Mutant with Only Two Mesophyll Cell Chloroplasts. *Plant Physiol* **106**: 1169-1177.

Redmon J and Farhadi A. 2016. YOLO9000: better, faster, stronger. 2016. *IEEE Conference on Computer Vision and Pattern Recognition (CVPR)*, 6517–6525.

Rueden CT, Schindelin J and Hiner MC. 2017. ImageJ2: ImageJ for the next generation of scientific image data. *BMC Bioinformatics* **18**:529.

Sakisaka M. 1929. On the number of chloroplasts in the guard cells of seed plants. Bot. *Mag* **43**: 46–48.

Schubert M, Petersson UA, Haas BJ, Funk C, Schröder WP and Kieselbach T. 2002. Proteome map of the chloroplast lumen of Arabidopsis thaliana. *J Biol Chem* **277**:

688 8354-65.
689 Schneider C A, Rasband W S and Eliceiri K W. 2012. NIH Image to ImageJ: 25
690 years of image analysis. *Nature methods* **9**: 671-675.
691 Simonyan K, Zisserman A. 2014. Very Deep Convolutional Networks for Large-
692 Scale Image Recognition. *CoRR* abs/1409.1556.
693 Song Y, Feng L, Alyafei MAM, Jaleel A and Ren M. 2021. Function of Chloroplasts
694 in Plant Stress Responses. *Int J Mol Sci* **22**: 13464.
695 Ukwueze CK, Oselebe HO and Nnamani CV. 2022. Ploidy determination of Musa
696 germplasm using morphological descriptors and chloroplast count in pairs of
697 stomatal guard cells. *Nigerian Journal of Botany* **35**: 161-172.
698 Van Valen, D. A., Kudo, T., Lane, K. M., et al. 2016. Deep learning automates the
699 quantitative analysis of individual cells in live-cell imaging experiments. *PLoS*
700 *Computational Biology* **12(11)**: e1005177.
701 van Wijk KJ, Peltier JB and Giacomelli L. 2007. Isolation of chloroplast proteins
702 from Arabidopsis thaliana for proteome analysis. *Methods Mol Biol* **355**: 43-8.
703 Wakasugi T, Nagai T, Kapoor M, Sugita M, Ito M, Ito S, Tsudzuki J, Nakashima K,
704 Tsudzuki T and Suzuki Y et al. 1997. Complete nucleotide sequence of the
705 chloroplast genome from the green alga Chlorella vulgaris: the existence of genes
706 possibly involved in chloroplast division. *Proc Natl Acad Sci U S A* **94**: 5967-72.
707 Wang CY, Bochkovskiy A and Liao HYM. 2023. YOLOv7: Trainable bag-of-
708 freebies sets new state-of-the-art for real-time object detectors. In Proceedings of
709 the IEEE/CVF Conference on Computer Vision and Pattern Recognition. 7464-
710 7475.
711 Whatley FR. 1975. Chloroplasts. Ciba Found Symp **31**: 41-61.
712 Watts A, Bondada R and Maruthachalam R. 2023. Identification of Arabidopsis
713 thaliana haploid plants by counting the chloroplast numbers in stomatal guard cells.
714 *Plant Physiology Reports*. 1-5.
715 Xie W, Noble JA and Zisserman A. 2018. Microscopy cell counting and detection

with fully convolutional regression networks. *Computer Methods in Biomechanics and Biomedical Engineering: Imaging and Visualization* **6**: 283-292.

Xiong D, Huang J and Peng S. 2017. A few enlarged chloroplasts are less efficient in photosynthesis than a large population of small chloroplasts in *Arabidopsis thaliana*. *Sci Rep* **7**: 5782.

Zahra N, Al Hinai M. S, Hafeez M. B et al. 2022. Regulation of photosynthesis under salt stress and associated tolerance mechanisms. *Plant Physiology and Biochemistry* **178**, 55-69.

Guan H, Xu X, He C, et al. (2016). Fine mapping and candidate gene analysis of the leaf-color gene ygl-1 in maize. PLoS One, 11(4), e0153962.

Kong, S. G., Suetsugu, N., Kikuchi, S., et al. (2013). Both phototropin 1 and 2 localize on the chloroplast outer membrane with distinct localization activity. *Plant and Cell Physiology*, 54(1), 80-92.

Supporting information

Extended data (including 10 Supplementary Figures and 1 Supplementary table) is available for this paper.

Fig. S1 The leaf of the three plant materials used for chloroplast detecting and counting.

Fig. S2 Detection results of the extended experimental data using the YOLOv7-D&Cchl model.

Fig. S3 Network structure diagram of Yolov7 algorithm

Fig. S4 Detailed Detection and Evaluation of Chloroplasts in Microscopic Plant Cells

Fig. S5 Detailed Detection and Evaluation of Chloroplasts in Microscopic Plant Cells

Fig. S6 Feasibility Analysis of 3D Chloroplast Detection

Fig. S7 Precision Curve

744 **Fig. S8** Recall Curve

745 **Fig. S9** F1 Score Curve

746 **Fig. S10** 3D Single-Cell Detection Analysis

747 **Table S1** Test Image Information and Sources

748

749 **Figure Legends**

750 **Fig. 1 Workflow of the YOLOv7-D&Cchl for chloroplast detection and**
751 **counting. (a)** Detailed steps for chloroplast detection using YOLOv7. Microscopic
752 images of plant cells are initially collected and labeled using the **labelImg** tool. This
753 data can be further divided into training and validation sets to train the **D&Cchl**
754 model. Additionally, manually annotated data is used for comparison with the
755 model's predictions. **(b)** Strategy and procedure for chloroplast detection and
756 counting in 3D model generated from muti-layer stack. Five images from different
757 focal planes are selected as input, and the **Intersection over Union** (IOU) strategy
758 is integrated to avoid double counting, ensuring accurate counting of chloroplasts
759 throughout the sample. **(c)** Process for ensuring chloroplast counting on individual
760 cells using the **Cellpose** model. Muti-layer images are initially fed into the model
761 for cell segmentation. Subsequently, these segmented images are passed through
762 the trained **D&Cchl** model to complete chloroplast detection. Blocks colored in
763 gray represent the dataset, yellow represents software, blue represents the neural
764 network framework, and dark green represents the models generated from the
765 training process.

766

767 **Fig. 2 Assessment of the YOLOv7-D&Cchl Model. (a)** The sample distribution
768 for S.squ includes three images containing 31, 31, and 29 chloroplasts respectively,
769 while for P.pat, the images contain 55, 58, and 57 chloroplasts respectively. **(b)** The
770 precision-recall curve, effectively highlighting the model's exemplary performance
771 in both precision and recall. Notably, at a classification threshold of 0.5, the model

achieves a precision of 87.7%. **(c)** A composite view of our samples and the detection results from the YOLOv7-D&Cchl model. **(d)** The original images, the images processed by the model, and manual annotations, vividly illustrating the strengths and potential limitations of the model. Specifically, the white dashed boxes emphasize the challenges faced by the model when focusing on chloroplasts located at different positions.

Fig. 3 Chloroplast Detection and Counting in 3D Volume. (a)-(c) The microscopic image series and their chloroplast detection results for *Sphagnum squarrosum* (*S. squ*), *Physcomitrium patens* (*P. pat*), and *Ricciocarpos natans* (*R. nat*), respectively. Slice1 to 5 represents the first to the fifth layer of chosen image from each respective sample's microscopic image series, where all detected chloroplasts have been incorporated into the corresponding benchmark. Scale bars represent 10 μm.

Fig. 4 Applications of 3D volumetric detection using the YOLOv7-D&Cchl model across different image types. (a) 3D chloroplast detection in fluorescent *Arabidopsis thaliana* [*A.tha*], with a total of 66 chloroplasts detected. **(b)** 3D chloroplast detection in electron microscopy images of *Sphagnum squarrosum* [*S.squ*], revealing 5 chloroplasts. **(c)** 3D chloroplast detection in *Wolffia arrhiza* [*W.arr*], identifying 73 chloroplasts. These images were tested using the YOLOv7-D&Cchl_F, YOLOv7-D&Cchl_E, and YOLOv7-D&Cchl_L models, respectively.

Fig. 5 Chloroplast Detection and Counting within Single 3D Cells. (a) Single cell segmentation via Cellpose towards single-layer image. The single cells are marked with numbers, and the complete ones were selected for analysis. **(b)** Chloroplast detecting and counting via YOLOv7-D&Cchl in single layer images. **(c)** Single cell segmentation via Cellpose towards muti-layer image (forming a 3D

structure). **(d)** Chloroplast detecting and counting via YOLOv7-D&Cchl in the muti-layer images. For **(b)** and **(d)**, No.Chl means the number of chloroplast detected. The red boxes mean the detected targets.

Fig. 6 D&Cchl performance on external public data. The first row shows the randomly selected input images without preprocessing, and the second row presents the corresponding output images where the detected chloroplasts are highlighted. These results validate the robustness and universality of our proposed chloroplast counting method on new data.

Fig.7 Overview of Chloroplast Counting Techniques Development. (a) Overview of major methods for chloroplast counting, from manual to our proposed 3D single-cell detection. **(b)** Process of chloroplast detection in 2D cells; **(c)** Workflow for chloroplast detection in 3D cells using multi-focal plane imaging and deep learning.

Table 1 A comprehensive comparison of chloroplast detection and counting methods

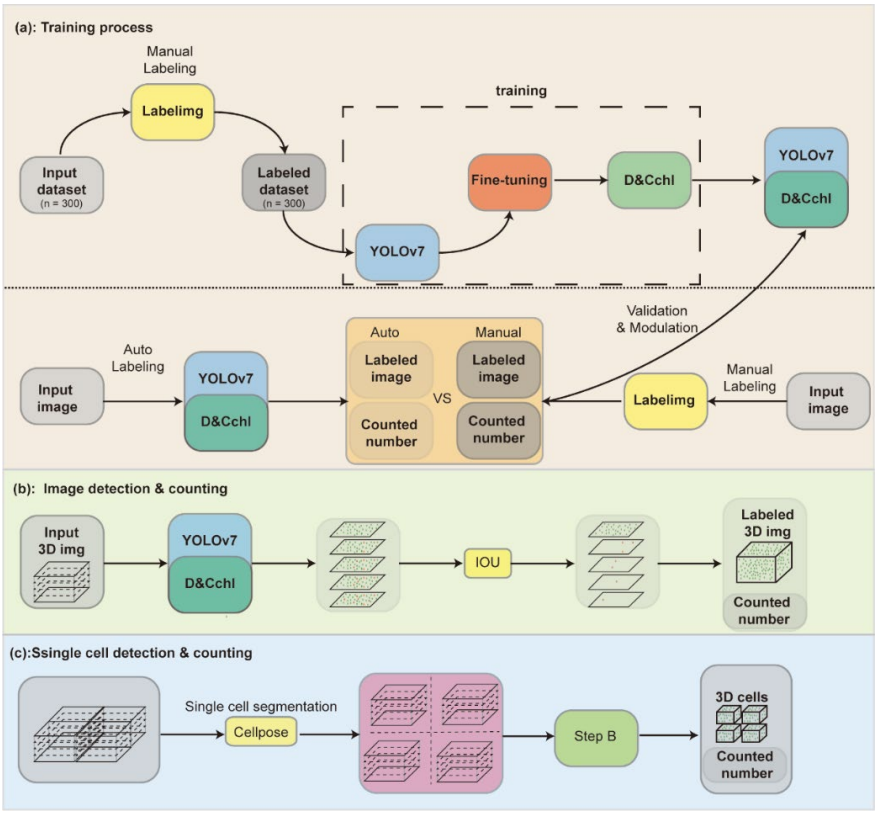

Fig. 1 Workflow of the YOLOv7-D&Cchl for chloroplast detection and counting. (a) Detailed steps for chloroplast detection using YOLOv7. Microscopic images of plant cells are initially collected and labeled using the **labelImg** tool. This data can be further divided into training and validation sets to train the **D&Cchl** model. Additionally, manually annotated data is used for comparison with the model's predictions. **(b)** Strategy and procedure for chloroplast detection and counting in 3D model generated from muti-layer stack. Five images from different focal planes are selected as input, and the **Intersection over Union** (IOU) strategy is integrated to avoid double counting, ensuring accurate counting of chloroplasts throughout the sample. **(c)** Process for ensuring chloroplast counting on individual cells using the **Cellpose** model. Muti-layer images are initially fed into the model for cell segmentation. Subsequently, these segmented images are passed through the trained **D&Cchl** model to complete chloroplast detection. Blocks colored in gray represent the dataset, yellow represents software, blue represents the neural network framework, and dark green represents the models generated from the training process.

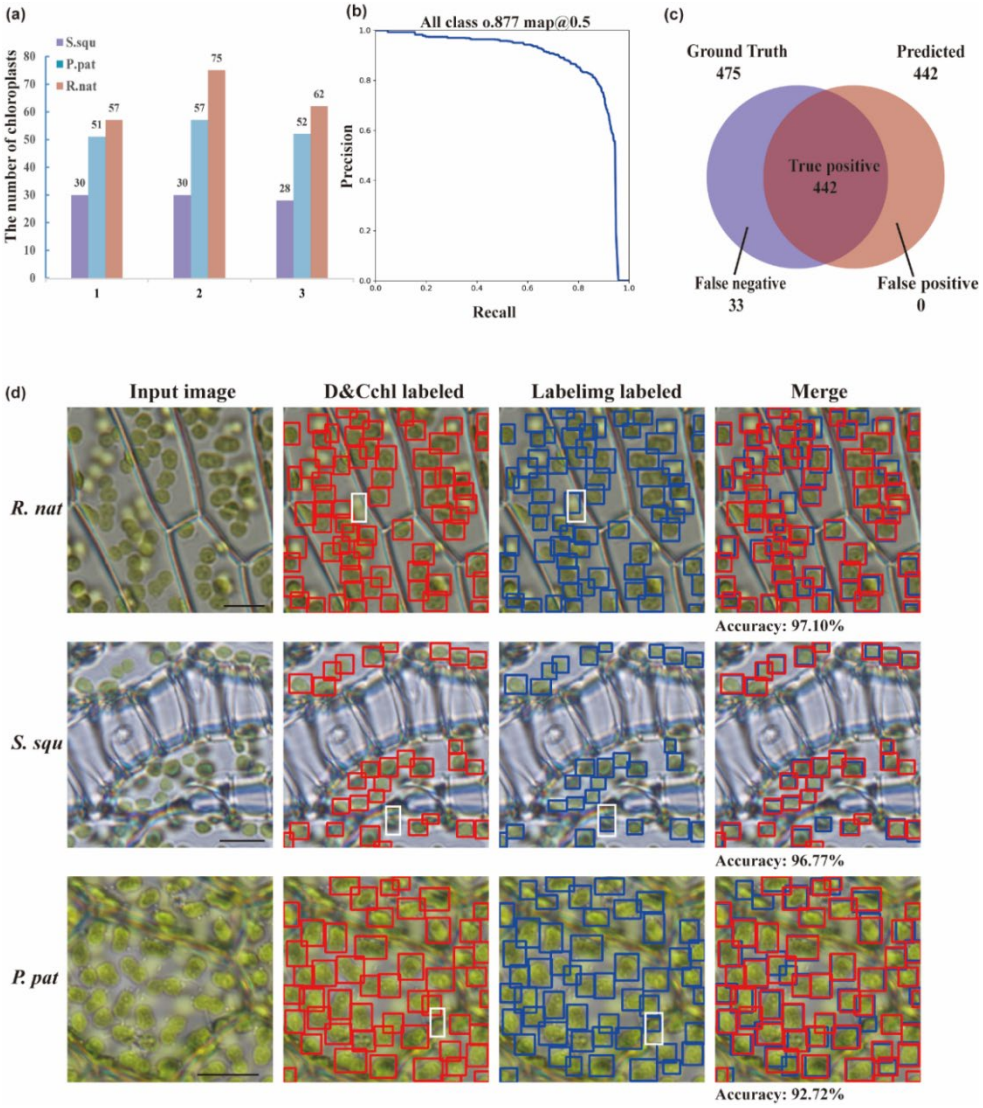

836

837 **Fig. 2 Assessment of the YOLOv7-D&Cchl Model. (a)** The sample distribution
838 for S.squ includes three images containing 31, 31, and 29 chloroplasts respectively,
839 while for P.pat, the images contain 55, 58, and 57 chloroplasts respectively. **(b)** The
840 precision-recall curve, effectively highlighting the model's exemplary performance
841 in both precision and recall. Notably, at a classification threshold of 0.5, the model
842 achieves a precision of 87.7%. **(c)** A composite view of our samples and the
843 detection results from the YOLOv7-D&Cchl model. **(d)** The original images, the
844 images processed by the model, and manual annotations, vividly illustrating the
845 strengths and potential limitations of the model. Specifically, the white dashed
846 boxes emphasize the challenges faced by the model when focusing on chloroplasts
847 located at different positions.

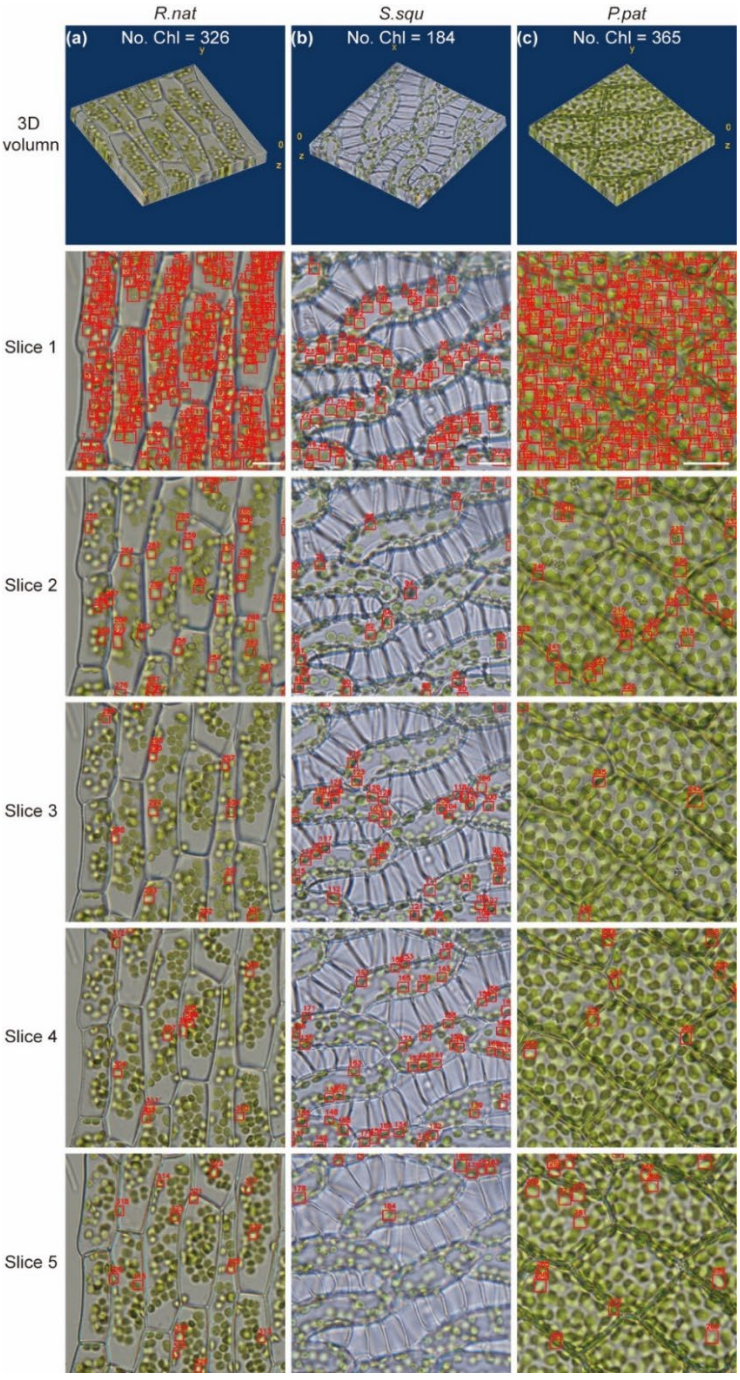

Fig. 3 Chloroplast Detection and Counting in 3D Volume. (a)-(c) The microscopic image series and their chloroplast detection results for *Sphagnum squarrosum* (*S. squ*), *Physcomitrium patens* (*P. pat*), and *Ricciocarpos natans* (*R. nat*), respectively. Slice1 to 5 represents the first to the fifth layer of chosen image from each respective sample's microscopic image series, where all detected chloroplasts have been incorporated into the corresponding benchmark. Scale bars represent 10 μm.

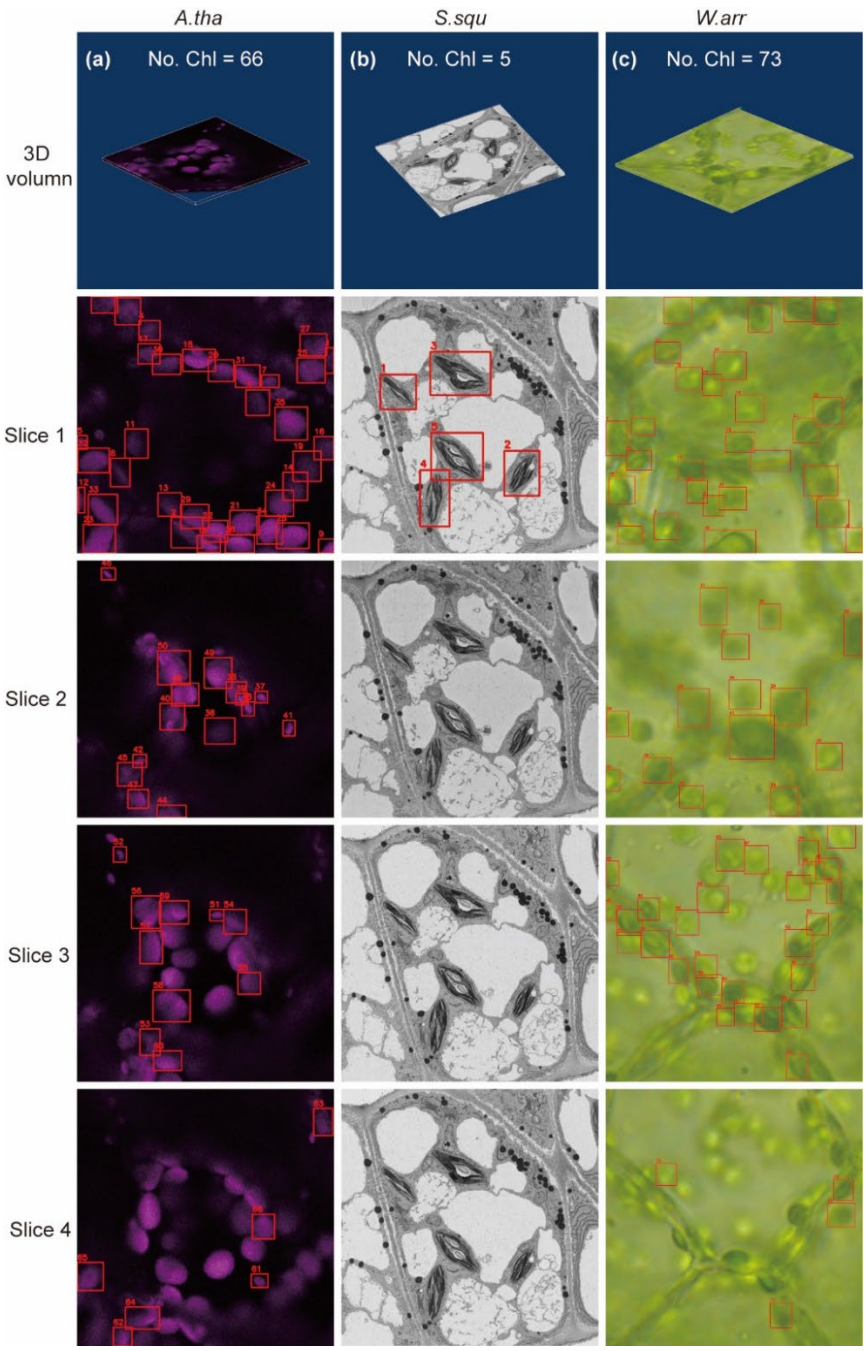

Fig. 4 Applications of 3D volumetric detection using the YOLOv7-D&Cchl model across different image types. (a) 3D chloroplast detection in fluorescent *Arabidopsis thaliana* [*A.tha*], with a total of 66 chloroplasts detected. **(b)** 3D chloroplast detection in electron microscopy images of *Sphagnum squarrosum* [*S.squ*], revealing 5 chloroplasts. **(c)** 3D chloroplast detection in *Wolffia arrhiza* [*W.arr*], identifying 73 chloroplasts. These images were tested using the YOLOv7-D&Cchl_F, YOLOv7-D&Cchl_E, and YOLOv7-D&Cchl_L models, respectively.

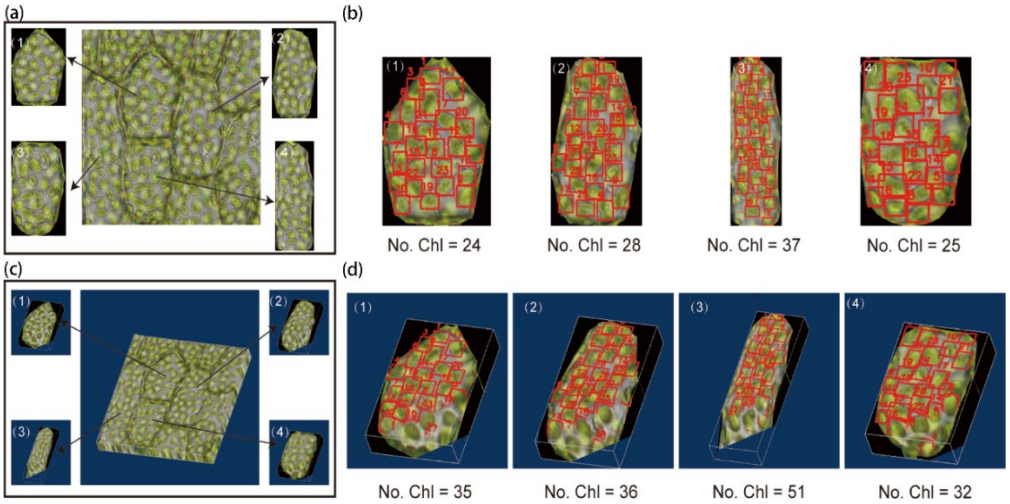

Fig. 5 Chloroplast Detection and Counting within Single 3D Cells. (a) Single cell segmentation via Cellpose towards single-layer image. The single cells are marked with numbers, and the complete ones were selected for analysis. **(b)** Chloroplast detecting and counting via YOLOv7-D&Cchl in single layer images. **(c)** Single cell segmentation via Cellpose towards muti-layer image (forming a 3D structure). **(d)** Chloroplast detecting and counting via YOLOv7-D&Cchl in the muti-layer images. For **(b)** and **(d)**, No.Chl means the number of chloroplast detected. The red boxes mean the detected targets.

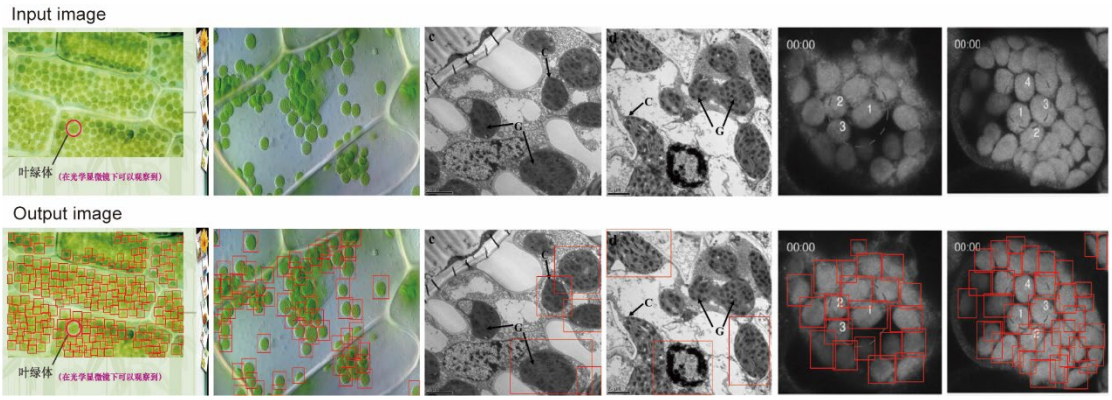

Fig. 6 D&Cchl performance on external public data. The first row shows the randomly selected input images without preprocessing, and the second row presents the corresponding output images where the detected chloroplasts are highlighted. These results validate the robustness and universality of our proposed chloroplast counting method on new data.

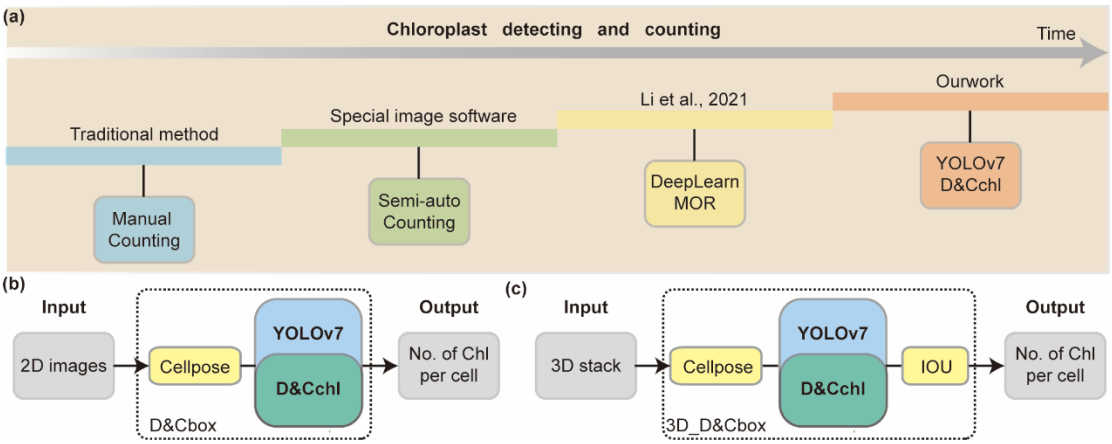

Fig. 7 Overview of Chloroplast Counting Techniques Development. (a) Overview of major methods for chloroplast counting, from manual to our proposed 3D single-cell detection. **(b)** Process of chloroplast detection in 2D cells; **(c)** Workflow for chloroplast detection in 3D cells using multi-focal plane imaging and deep learning.

Table1 A comprehensive comparison of chloroplast detection and counting methods

Counting method	Scope of observation	Staining (Yes/No)	Live Cell (Yes/No)	References
Manual	2D Slice	No	Yes	Lutz and Dzik,1993
Semi-auto	2D Slice	No	Yes	Arena, 2017
DeepLearn MOR	2D Slice	Yes	No	Li et al., 2021
YOLOv7 D&Cchi	3D, whole cell	No	Yes	This study